FORMULATION DESIGN AND DEVELOPMENT OF BENTONITE INCORPORATED TRIMETAZIDINE OPHTHALMIC DELIVERY

Introduction

Ocular diseases, such as glaucoma, conjunctivitis, diabetic retinopathy, and cataract, are prevalent worldwide and significantly impact the quality of life for affected individuals. These conditions can lead to vision loss or blindness. The high prevalence and impact of ocular diseases make them a priority for research and development of effective treatment.

Oxidative stress plays a vital role in developing many ocular complications, such as cataracts, glaucoma, diabetes retinopathy, macular degeneration, uveitis, etc. In oxidative stress, an excess amount of reactive oxygen species (ROS) generated lead morphological and functional impairments in retinal ganglionic cells (Hironaka et al., 2011; Masuda et al., 2017). Ocular inflammation (uveitis) is an inflammation of the uvea, the central layer of the eye that includes the iris, ciliary body, and choroid. Additionally, the retina and vitreous humour of the eye may be impacted. Ocular inflammation is a dangerous illness that has to be treated quickly and effectively. Significant pain, redness, sensitivity to light (photophobia), and discomfort may all be symptoms of ocular inflammation. Treatment seeks to lower inflammation, ease symptoms, and raise the patient's level of comfort in general (Durand, 2015). Ocular inflammation may cause several problems, including glaucoma (increased intra ocular pressure within the eye), cataracts (clouding of the lens of the eye), macular edema (swelling in the middle of the retina), and retinal detachment. These problems might result in further operations or surgeries and significant harm to the eyes. To lessen the likelihood of adverse effects, ocular inflammation may be rapidly and successfully treated (Hu et al., 2011).

Glaucoma is a leading cause of irreversible vision loss, with over 80 million people in 2020 currently affected globally. As per the World Glaucoma Association, the number is

expected to reach 111.8 million in 2040. Glaucoma is a multifactorial neurodegenerative disorder with several forms that may cause irreversible vision loss and damage to both the optic nerve axons and retinal ganglion cell (Tezel, 2021). Open angle glaucoma (OAG) is associated with increased intraocular pressure (IOP). Thus, the treatment of glaucoma focused on lowering IOP. Endothelin-1 (Et-1) is synthesized and secreted in a three to four times higher in the aqueous humour compared to healthy human plasma (Rosenthal and Fromm, 2011). ET-1 participates in IOP regulation by constricting the trabecular meshwork contractility. So IOP affected by elevated ET-1 in aqueous humour of glaucoma patient as compared to a normal human (Choritz et al., 2012). Many studies have been proved an increasing ET-1 in aqueous humour causes an elevation in IOP. A study using the Morrison rat model of glaucoma found that increased IOP leads to elevate the ET-1 level 2 to 2.5 folds in aqueous humour (Zhang et al., 2003a). Further evidence from a 2010 study found ET-1 is a significant component for the elevation of IOP by using capillaries of rat retina (Rigosi et al., 2010).

Many reports have already presented earlier on protective action of trimetazidine against retinal ischemia after intraperitoneal (Mohand-Said et al., 2002) and oral (Nowak et al., 2007) administration. Trimetazidine dihydrochloride have a short elimination half-life of 3 to 4 h which leads to repeated administration (2-3 times daily).

Ocular drug delivery is a challenging work for scientists to achieve acceptable therapeutic drug concentrations at the targeting eye tissues. Eye drops are the most common formulations in ocular delivery systems. However, only 1-10% of the drug is absorbed, with the majority being removed from the precorneal region. Short precorneal residence time, tear turnover, and reflex blinking are amongst the major causes of poor ocular bioavailability.

Polymer-clay composites have generated a lot of attention in the field of drug delivery due to their unique features and advantages. Based on the unique layered structure,

intercalation property, high retention capacities as well as swelling bentonite have been proposed as very useful materials for modulating drug delivery. The clay component serves as a reservoir, allowing the drug to be controlled release over a prolonged period of time. By changing the composite's structure and content, the release rate can be tailored. The layered structure of clay minerals acts as a barrier against external factors like light, moisture, and temperature that may be able to damage the drug molecules, giving them great stability and the ability to prevent pharmaceuticals from deterioration or premature release. Polymer-clay composites can improve the bioavailability of drugs that are poorly soluble. The clay component can serve as a carrier and improve the solubility and absorption of hydrophobic drugs in the body. Targeted drug delivery can be achieved by polymer-clay composite. The modified polymer can respond to specific stimuli, such as temperature, pH, or enzyme, allowing the controlled release of the drug at the target site (Abdeen and Salahuddin, 2013).

Objectives

1. To develop bentonite clay-based film formulation for the topical delivery of trimetazidine to control ocular pressure. The effect of bentonite concentration on the release and permeation of trimetazidine is aimed to study. Determination of intraocular pressure after application of film formulation in normotensive rabbit eye model is aimed to be evaluated. The area under the decreased IOP versus time curve to be plotted to represent the sustained drug release of topical administered polymeric matrix formulation containing bentonite. Ternary molecular docking of trimetazidine-HPMC- bentonite is performed to observed stable interactions.

2. To develop a HPMC-poloxamer based sol-to-gel formulation containing bentonite for ocular anti-inflammatory effect of trimetazidine prophylactically. The aim is to achieve sustained and control ocular delivery of trimetazidine by incorporating bentonite

nanoplatelets into the formulation. Anti-inflammatory efficacy of the developed formulation is to be evaluated using a carrageenan-induced rabbit eye model.

3. To investigate the cytoprotective role of trimetazidine on carrageenan-induced ocular cell damage in a rat-eye model using hydrogel-forming film. Also aimed to carried out thiobarbituric acid reactive substance (TBARS) assay and histological study of rat eye for examining cytoprotective effect of trimetazidine. The current study also focused to investigate the protective effect of drug in a glucose-induced in-vitro cataract model on isolated goat-eye lens after topical application.

Materials and Methods

Animal

Nine New Zealand white rabbits (1.5-2.5 Kg) free from ocular abnormalities, including glaucoma, were used in this study. This study was approved by IAEC (Institutional animal ethics committee) with protocol no IAEC/SPS/SOA/21/2019. Animals were housed in the animal house of the School of pharmaceutical sciences Redg no.1171/PO/RE/S/08/CPSEA under-maintained standardized condition (twelve hours light-dark cycle), regulated air temperature (15-21 °C) and good ventilation. The animals were fed standard feed and had free access to water.

Materials

The active compound trimetazidine dihydrochloride was collected from Medley Research Center (Mumbai, Maharashtra). Polxamer 407 and Hydroxylpropyl methylcellulose (HPMC K 15M) were kindly provided by Ready's Laboratory (Hyderabad, India). Bentonite, triethanolamine and NaCl were purchased from HIMEDIA (Mumbai, India), SRL Pvt. Ltd. Mumbai, Merck Pvt Ltd (Maharashtra India) respectively. Other reagents used were of analytical grade.

Fabrication of trimetazidine ocular film

Treatment of Bentonite

Pre-treatment of the bentonite was performed after dispersing bentonite (100gm/L: solid/liquid ratio) into 0.2mol/L NaCl solution and shaking at 200rpm for 12-15 h. Bentonite was washed 5-6 times with double distilled water through centrifugation for removing excess chloride ions. Removal of chloride in the washings was confirmed by silver nitrate testing. Remaining bentonite slurry was dried immediately in a hot air oven at 60 °C and the dried sodium bentonite was preserved in a closed container till used for film preparation (Alshabanat et al., 2013).

Ocular film Formulation

Bentonite was dispersed (1% wt/vol) in double distilled water and continuously stirred at room temperature for 24 h. The bentonite dispersion was transferred in a separating funnel and allowed to stand for overnight period for settling of larger particles. The upper layer dispersion was collected carefully and centrifuged (2500 rpm) for 30 min. Then the upper thin dispersion was cautiously removed and used to prepare the film. The film was prepared by casting and solvent evaporation method. Swelling of HPMC K 15 M was done in presence of little amount of water and placing in the refrigerator for overnight period of about 12 h. The swelled gel was stirred magnetically for about 3 h and the thin bentonite dispersion was added into it with continuous stirring for another 24 h. Trimetazidine and triethanolamine were dissolved in a tiny quantity of water and added to the bentonite-HPMC dispersion and stirred for about 2 h. Then the prepared hydrogel was poured uniformly on a petri plate (Tarsons, diameter: 90 mm) and left for drying at 40 ◦C in an incubator for 24 h until constant weight was achieved. Folding endurance was conducted by folding a peace of film repeatedly at the same position up to 200 times or till it was broken. The surface pH of the film was measured by dipping the pH meter's glass electrode inside the swelled portion of the film formulation Table-1.

Formulation	HPMC (mg)	Drug/Bentonite ratio	Triethalonamine (%)	Thickness (µm) (mean±sd; n=6)	Folding endurance (n=6)	Permeation vs. drug release: Regression equation (r^2)
TB_0	1000	Bentonite-nil	15	86.83333 ±8.060	>200	y = 64.426x - 1314.9 R^2 = 0.9605
TB_1	1000	1: 10^{-4}	15	294.8333 ±17.611	>200	y = 52.146x + 249.08 R^2 = 0.9625
TB_2	1000	1: $2*10^{-5}$	15	200.8333 ±22.675	>200	y = 54.759x - 258.47 R^2 = 0.9947
TB_3	1000	1: 10^{-5}	15	134.3333 ±9.521	>200	y = 49.842x - 125.69 R^2 = 0.9969
TB_4	1000	1: $5*10^{-6}$	15	113±7.899	>200	y = 50.229x + 3.8837 R^2 = 0.9974
TB_5	1000	1: $2*10^{-6}$	15	99.5±11.040	>200	y = 63.296x - 557.97 R^2 = 0.968

Table-1: Bentonite incorporated HPMC film formulation for trimetazidine ophthalmic delivery.

Preparation of sol

TRZ in-situ gel based on POL was prepared using a slightly modified cold method. First, the required amount of HPMC and POL were dissolved in cold distilled water with continuous stirring for about 2 h. Then, thin dispersion of bentonite was added over the above mixture as per formulation tabulated in Table 2. Next, TRZ solution was added and stirred continuously for 1 h to get the homogenous sol preparation to make the final concentration of 20 mg per ml. Sol preparation of 5 ml was filled in a glass vial and well-closed (Aluminium cap sealed) vials were autoclaved at 121 °C for 20 min (15 psi) for final sterilization.

Gel code	HPMC (% w/vol)	POL (% w/vol)	Drug: Bentonite	pH	$T_{sol-gel}$ (°C)
TgB_0	0.2	17	Bentonite nil	6.8	33
$TgB_{2.0}$	0.2	17	1: $2*10^{-5}$	6.8	32
$TgB_{1.0}$	0.2	17	1: 10^{-5}	7.0	32
$TgB_{0.5}$	0.2	17	1: $5*10^{-6}$	7.2	32

Table 2-Bentonite containing aqueous in-situ gel formulation for ophthalmic delivery of trimetazidine

Gelling temperature, clarity, and pH

A test tube with about 1 ml of sol preparation was placed in a temperature-controlled water bath. A thermometer dipped in a second test tube containing 1 ml water was used as control for measuring gelling temperature. Temperature of the water bath was increased gradually, and the temperature at which the sol stopped flowing at its inverted state was recorded as sol-to-gel transformation (T1). Then gradually reduced the temperature and the temperature at which the gel began to flow again was recorded as gel-to-sol transformation (T2). The critical gelation temperature ($T_{sol-gel;}$ °C) was the average of T1 and T2. One of the major characteristics of ophthalmic preparations is clarity. Under a good light source and against a black-and-white background, the sol preparations were examined for their physical appearance and optical clarity. Calibrated pH meter (Systronics digital pH meter 335) was used to investigate the pH of the sol.

FTIR

The pure TRZ and formulations were scanned for IR transmission spectra to observe the drug-excipients interaction study. With an average of 80 scans and resolution of 4 cm^{-1}, the scans were performed in the range of 4000-600 cm^{-1}. In the FTIR spectrophotometer (JASCO

FT/IR 4600) the samples were placed above diamond ATR (JASCO ATR PRO ONE) crystal

Calorimetry analysis

DSC analysis of trimetazidine and the formulations were carried out by differential calorimeter (DSC-1, Mettler Toledo; Software- Star E, SNR- 18289) within a range of 30–300 ◦C in a constant heating rate of 10 ◦C/ min under continuous nitrogen purge (50 ml/min).

X-ray difraction

Diffraction patterns of pure trimetazidine, bentonite and the prepared films were performed by X-ray powder diffraction (Model: Rigaku, Ultima IV). For X-ray source, K-Alpha anode has been used with a voltage of 40Kv and 15mA current. The scanning was done in the 2Ɵ range of 5 to 70° with a scanning speed of 1^0 per min.

Rheology

A parallel plate rheometer (Mars III, Thermo Fisher Scientific, Germany) was used to evaluate the rheological behavior of sol formulation. For all evaluations, parallel plate geometry was used, with a diameter of 40 mm. Two types of rheological testing were carried out.

Steady shear deformation

The shear rate (γ) was changed in logarithmic scale from 0.01 to 2000 s^{-1} for the determination of viscosity and stress.

Oscillatory deformation (Frequency sweep)

The storage modulus (G′) and loss moduli (G′′) were determined by varying frequency from 0.01 to 100 Hz at a constant amplitude of deformation ($\gamma A \approx 0.1$ %).

Scannning electron microscopy

For surface morphology visualization, SEM analysis has been done. Pure powdered drug, films and sol formulations were sputter coated with platinum for 60 seconds in a vaccum

chamber followed by SEM analysis by applying a voltage of 5 to 15kv (Model: JEOL JSM-6510).

In-vitro drug release study

Prepared trimetazidine films were cut into suitable pieces, weighed and glued to the glass slides by using cyanoacrylate adhesive and dipped into the dissolution vessels containing phosphate buffer (200 ml, pH 7.4) in a USP type II dissolution tester (Electrolab, TDT06L, India). The peddle agitation was fixed to 50 rpm with the temperature at 34.0 ± 2 °C. Samples were withdrawn at a preset time interval and estimated spectrophotometrically at λ_{max} 269 nm after filtering through a 0.45 µm syringe driven filter. The drug diffusion study of the sol formulations were carried out using a modified Franz diffusion apparatus followed by the above mentioned condition.

Ex-vivo corneal permeation study

Fresh goat eye balls were procured from slaughter house within an hour after sacrifice and washed properly with distilled H_2O followed by phosphate buffer pH 7.4. The cornea along with an attached 5–6 mm broad sclera ring was removed from the whole goat eye. After placing a pre-weighed circular film to the centre of the epithelial cornea and positioning it in the diffusion chamber with an effective surface area of 1.56 cm2 facing the donor compartment. The diffusion media (phosphate buffer, pH 7.4, 200 ml) was put in the receptor compartment. The corneal permeation was kept going for 6 h at 34 ± 2 ◦C under steady agitation of 50 rpm 10 ml of samples were withdrawn as predetermined time and filtered through a 0.45 µm membrane filter and assayed by Ultra-Violet visible spectrophotometer (JASCO V-630 spectrophotometer, Software: Spectra Manager) at 269 nm. The experiment was performed triplicate and mean ± sd were calculated.

Kinetics

There were different kinetics models were used in previous reports to understand the mechanism of drug release and permeation from polymeric formulations. The Higuchi and Korsmeyer-Peppas equation was used to calculate the kinetics of percentage release and quantity penetration of trimetazidine dihydrochloride in the presence of bentonite.

Higuchi:

$Q=K_H \times \sqrt{t}$

Korsmeyer–Peppas

$$\frac{M_t}{M_\infty} = K_P \times t^n$$

Q = Cumulative amount of drug release, KH = Higuchi release rate constant/permeation rate constant, Mt = Amount of trimetazidine release/permeation at time t, M∞ = maximum amount of trimetazidine available to release/permeation, KP = parameter reflecting the structural and geometrical characteristics of the delivery device, or Peppas release/permeation rate constant, n = power law exponent, or release/ permeation exponent. The n value reflects drug release/permeation as regulated by Fick's laws and confirmed by Higuchi model. Both the Higuchi and Korsmeyer- Peppas equations were used to calculate the rate constants (KH and Kp) of dissolution and permeation, as well as the coefficient of determination (r^2). The differences in permeability coefficients between the control category of film without bentonite and the other categories of film with bentonite were investigated using one-way analysis of variance (ANOVA) in XLSTAT 2021 and the statistical significance was determined by a p value of less than 0.05. A double-sided Dunnett's analysis was used to compare the control (TB0) to the other films (TB1, TB2, TB3, TB4, TB5).

IOP experimental protocol

The rabbits were allocated into three groups (3 rabbits each) for studying the effect of topically applied trimetazidine drop, TZ film formulation with bentonite (TB3) and without

bentonite (TB0) on the normal IOP, respectively. The rabbits were kept in a restriction cage for IOP measurements. 30 minutes before starting the experiment, rabbits were anaesthetized with 0.5% tetracaine HCl (0.75 mg in 150 µl) and a control or zero time value of IOP was recorded. One drop of freshly prepared TZ was instilled in the middle of the inferior conjunctival sac, followed by lid closure. In another two groups, TZ films (TB0 and TB3) were applied into the cul-de-sac region of the rabbit eye shown in Figure 4 (A) IOP was measured using a Schiotz Tonometer (Riester, Germany) is placed on the cornea shown in Figure 4 (B) Conversion of the scale value into table value provided by the manufacturer calculates the IOP in mmHg units. All values repeated thrice and are presented as mean ± SE. After completion of the experiment, eyes were washed properly with normal saline followed by moxifloxacin eye drop.

Anti-inflammation study

For evaluation of anti-inflammatory effect, the standard carrageenan-induced rabbit eye model was used without sacrifice. Male New Zealand rabbits were separated into 3 groups containing three each. Group I was treated as the test group (with formulation), Group II was positive control group- (Carrageenan induced), and Group III was treated as negative control group. For anti-inflammation study, sol formulation was instilled in Group-I (50 µl; 1 mg/Kg) and 2 h after the same animals received carrageenan injection subconjunctivally (200 µl; 2 % w/v). Group-II rabbits received carrageenan injection (same dose). Photographs were taken of any signs of acute inflammation and reddening of the conjunctiva, followed by lachrymal secretions. After the completion of the experiment of about 4 h Moxifloxacin Eye Drop I.P (0.5 % w/v) was instilled in the eye for quick recovery.

Computational analysis

The computational research work was carried out in Linux-Ubuntu 16.04 LTS system. As per the requirements, the HPMC and Montmorillonite unit cell were designed using the software

MarvinSketch (ChemAxon, Budapest, Europe) from the previously published papers (Fini et al., 2017) and the drug, trimetazidine was retrieved from PubChem (CID: 83201) for this study. Further, all chemical structures were converted to pdb (.pdb) format with clean geometry using BIOVIA Discovery Studio Visualizer software (BIOVIA DSV). The software, AutoDock 4.1, was used for molecular docking study. The molecular interactions of single and double docking complexes were visualized using BIOVIA DSV (Swain et al., 2020).

Results & Discussion

OBJECTIVE-1

Properties of formulated film

Surface pH found (7.0–7.2) was very much compatible with the eye and supposed to produce no irritation. Film have also demonstrated good folding endurance and not brittle rather strong and plastic in nature to produce sufficient flexibility upon placing in the cul-de-sac due to the presence of triethalonamine.

FTIR

Figure 1 (A) shows IR spectra of trimetazidine, bentonite and film containing different amount of bentonite. The IR spectrum of Trimetazidine showed the characteristic bands of –CH stretching, -NH_2 bending, -OH stretching, -CH bending, -C-O stretching at 2923, 1600, 3489, 1415, and 1099 cm^{-1} respectively (Chiş et al., 2011).

The spectrum of pure bentonite Figure 1 (A) exhibited a broad band at 3420 cm^{-1} attributed to the –OH stretching mode of interlayer water. The characteristic band at 1638 and 1108 cm^{-1} indicate the bending vibration of physically adsorbed water and longitudinal Si-O stretching vibration respectively. The observed absorption band at 3622 cm^{-1} and 915 cm^{-1} associated with Al-OH and Mg-OH stretching and Al-Al-OH bending vibration are distinctive for dioctahedral smectite. The principal absorption bands appeared at 1033 cm^{-1} and 782 cm^{-1}

due to Si-O stretching of smectite and quartz, respectively. The bands at 534 and 789 cm^{-1} originated due to Fe-O-Si and Mg-Al-Oh respectively (Alshabanat et al., 2013).

For all formulations with trimetazidine, the characteristic vibration of –CH stretching was clearly observed around 2923 cm^{-1}. The relatively weak absorption around 1415 and 1600 cm^{-1} was assigned to the C-H bending and $–NH_2$ bending respectively. The absorption band at 1638 and 1108 cm^{-1}, due to OH deformational mode of water and the longitudinal Si-O stretching vibration for bentonite nanoclay also appeared in the spectra of the formulations. This is indicating the presence of trimetazidine and bentonite in clay containing complex. The broadening of absorption band in the range 3400-3200 cm^{-1} was observed due to the presence of polymer. Moreover, the band of at 1638 and 1033 cm-1 was broadened in the spectra of all formulations. These changes suggested to the interactions between the functional group of trimetazidine (amide) and the bentonite nanoclay (Zhang et al., 2020).

Differential scanning calorymetry

In Figure 1 (B) the calorimetry of pure trimetazidine showed a sharp melting endothermal peak at 236.13 ◦C with an onset of melting, 228.48 ◦C confirming its crystalline characteristics. Shifting of the endothermic melting peak with weaker enthalpy in the film formulations is a sign of nearly full amorphization of the drug crystals (El-Nahas and Hosny, 2011). It happens probably due to arresting of drug amorphous state in to the polymer-clay matrix (Panda et al., 2014). A broad endothermic peak in the range of 80–100 C has been found in all film formulations due to water evaporation in the HPMC matrix. A broad endothermic peak in the range of 80–100 ◦C has been found in all film formulations due to water evaporation in the HPMC matrix.

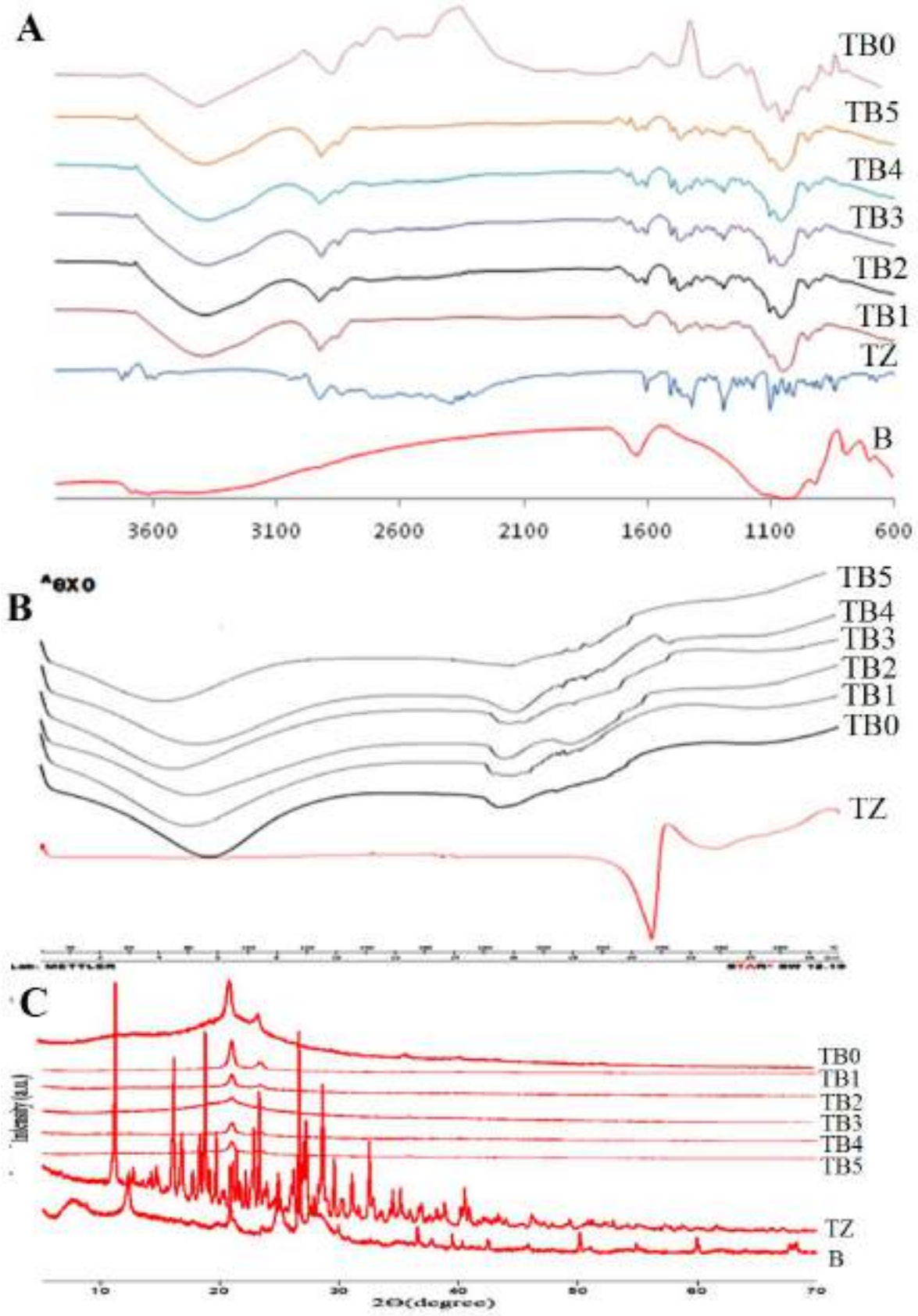

Figure 1 (A) FTIR spectrograms (B) DSC thermogram (C) XRD pattern of trimetazidine dihydrochloride and film formulation.

X-ray difractometry

In Figure 1 (C) the diffraction spectrum of Na-bentonite exhibited characterization peak at 2Ɵ 6.78(001) and 20.5 (110) peak of pure montmorillonite (Zhang et al., 2020). The deffractogram of pure drug showed the characteristic peak at 11.4, 15.5, and 18.9 (2Ɵ) indicating the crystalline pattern of trimetazidine. The majority of diffraction peak was disappeared may be due to the electrostatic attraction of the positively charged drug with the negatively charged surface of the clay and the –OH group of HPMC (Zhang et al., 2020). However, no diffraction peaks of trimetazidine were observed in the XRD profile of trimetazidine-loaded composites. It is supposed to be the drug was dispersed in the composites in molecular form, may be due to the electrostatic attraction of the positively charged drug with the negatively charged surface of the clay and the –OH group of HPMC. It was also observed that in presence of bentonite drug becomes more amorphised. The disappearance of characteristic peaks of the bentonite in film formulations suggested that, bentonite was amorphously distributed in the polymeric matrix (Zhang et al., 2020).

SEM

SEM images were utilised to study the surface morphology of pure trimetazidine, and films containing bentonite and without bentonite in Figure 2. The geometric nature of the trimetazidine crystal is distinctly noticed in Figure 2 (A). The crystal geometry of drug has almost been lost in the SEM of the film formulation in the presence and absence of the nano sized bentonite particles. SEM indicates that the high degree of dispersion of clay in the HPMC matrix was obtained at nano level of clay content when low concentration of clay content in Figure 2 (F-G). In increasing Bentonite concentration, dispersion becomes more difficult and more particles are agglomerates can be evidenced by Figure 2 (C, D, & E). It should be noted that, this behaviour is usual; because of higher concentration of nanoparticles

dispersion in to polymer matrix becomes difficult even under high shear force mixing condition (Savas and Hancer, 2015).

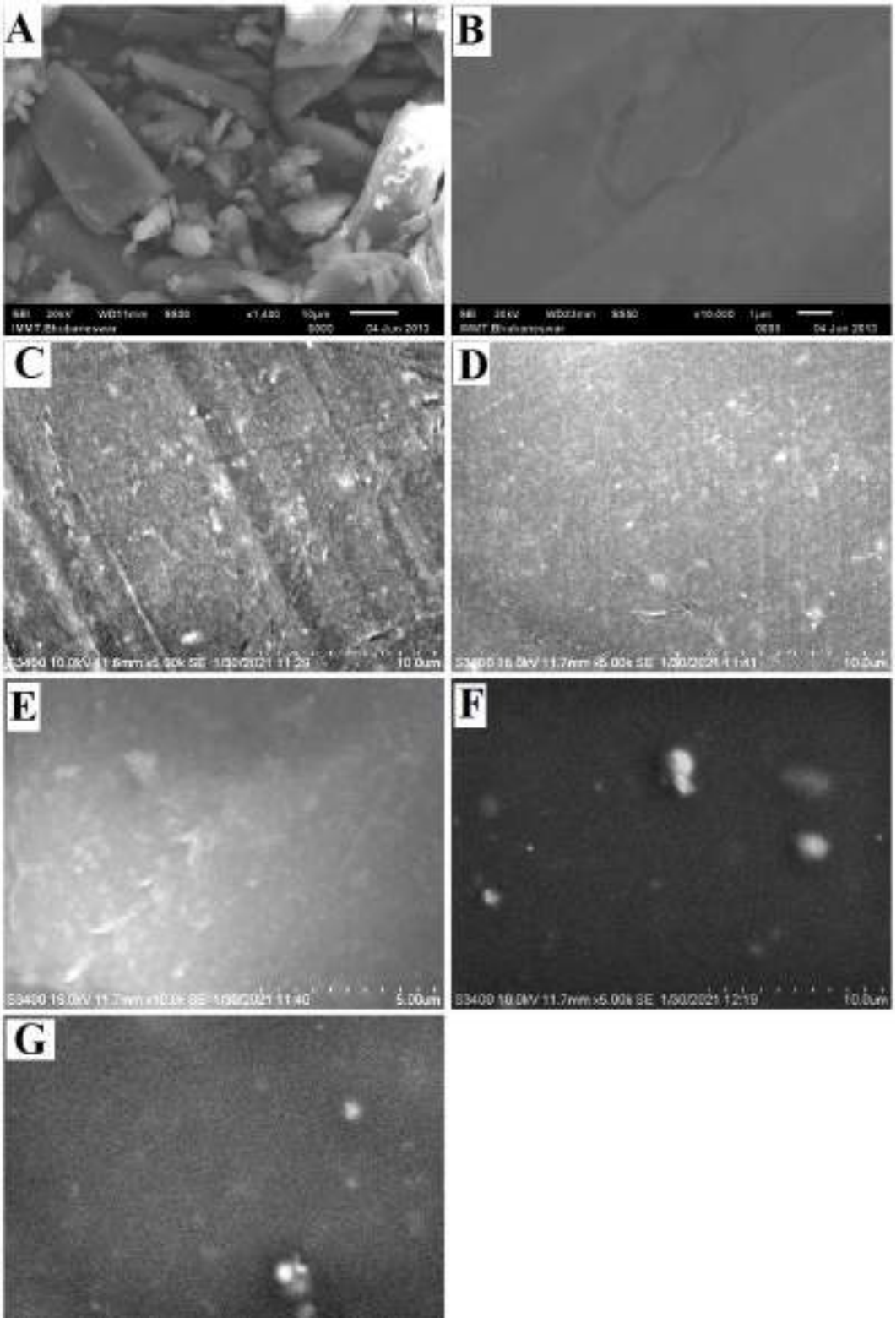

Figure 2 Scanning electron micrographs of pure drug crystals (A) and film formulations in HPMC K15 matrix TB0 (B), TB1 (C), TB2 (D), TB3 (E), TB4 (F), TB5 (G).

Drug dissolution testing

Drug dissolution experiment of TZ from bentonite incorporated HPMC films in simulated tear fluid (34 ◦C, pH 7.4) is shown in Figure 3 (A). When bentonite is not present in the film (TB0), the entire release of TZ is seen in 180 min. The drug release was extended up to 6 h along with the decreased bentonite amount. This finding can be attributed to TZ adsorption on the bentonite surface, which enabled cation exchange and hydrogen bonding between the surface –OH and –NH of TZ. The adsorption of atenolol on to Ca-montmorillonite surface has already been proved by cation exchange and hydrogen bonding via the NH group, benzene ring, COH groups of the atenolol molecule (Chang et al., 2019). Doxorubicin was found to be adsorbed effectively on the surface of bentonite nanoclay by forming electrostatic interaction and hydrogen bonding between NH group of doxorubicin and surface hydroxyl group of bentonite (Hosseini et al., 2018). Because of their tortuous diffusion paths, silicate-based polymer nanocomposites have strong barrier characteristics and can be utilised in the development of applications for sustained drug release. For TZ sustained release from the HPMC k15 M matrix, the following sequence was observed: TB0 > TB5 > TB1 > TB2 > TB4 > TB3. This observation demonstrates that the decreasing amount of bentonite should be in an appropriate ratio for optimal drug release. This suggests that a high concentration of bentonite would disrupt the production of a denser HPMC matrix film due to the –OH group in bentonite reacting with the hydrogen in the HPMC, disrupting the electrostatic connection between bentonite and TZ. As a result of these factors, TZ was released quickly from the film formulation (Zhang et al., 2020). To evaluate the release kinetics, the Higuchi and Korsmeyer-Peppas models were utilised. Estimated kinetic value of dissolution exponent (n), coefficient of regression (r2), and rate constant (K) were depicted in Table 3. According to Peppas model, $n < 0.5$ indicates the pattern of Fickian release. For all the formulations the n value was residing between 0.260 and 0.414 indicated the release pattern as diffusion.

Higuchi model fitting was also used to examine the diffusion-controlled release kinetics of all formulations (r2 = 0.910–0.989).

Table-3: Kinetic of in vitro drug release and ex vivo permeation.

	Release				Permeation					
	Higuchi		peppas		Higuchi		Peppas			
Film formulations code	K (% $min^{-½}$)	r^2	n	r^2	K (% $min^{-½}$)	r^2	n	r^2	Js (µg/min)	$P_{Film*10^{-5}}$ (cm/min)
TB0	6.333	0.910	0.260	0.969	5.643	0.983	0.402	0.997	60.022	6.2
TB1	5.100	0.970	0.414	0.991	4.233	0.983	0.366	0.994	19.43	5.70
TB2	4.900	0.970	0.343	0.999	4.137	0.984	0.359	0.996	17.9	5.12
TB3	4.102	0.976	0.356	0.996	3.609	0.980	0.323	0.988	13.85	2.59
TB4	4.855	0.989	0.367	0.995	3.978	0.984	0.356	0.998	15.97	3.72
TB5	5.191	0.941	0.331	0.991	4.612	0.981	0.381	0.996	36.585	5.74

Table-4 formulation / Dunnett (two sided) / Analysis of the differences between the control category formulation-TB0 and the other film formulation with a confidence interval of 95%:

Contrast	Difference	Standardized difference	Critical value	Critical difference	Pr > Diff	Significant
TB0 vs TB3	5.077	13.397	2.901	1.099	<0.0001	Yes
TB0 vs TB4	4.787	12.631	2.901	1.099	<0.0001	Yes
TB0 vs TB2	2.153	5.682	2.901	1.099	0.000	Yes
TB0 vs TB1	1.653	4.363	2.901	1.099	0.004	Yes
TB0 vs TB5	1.453	3.835	2.901	1.099	0.010	Yes

Ex-vivo corneal permeation

Ex vivo permeation was carried out more than 6 h using fresh goat cornea and the amount of TZ penetrated per unit area vs. time profiles are depicted in Figure 3 (B). Reduced bentonite concentration in the film formulation resulted in a lower rate of penetration into goat corneal tissue. The following order was observed for TZ permeation from the formulations: TB0 > TB5 > TB1 > TB2 > TB4 > TB3. The permeation kinetics were studied using Higuchi and Korsmeyer-Peppas. Table 4 illustrates the parameters. Peppas permeation exponent value (n) of all formulations were <0.5 (0.323–0.402) therefore, can be described as diffusion-controlled. The linearity of the Higuchi model also validated the formulation (0.980–0.984). The quantity penetrated per cm2 vs time profile plot was used to calculate the permeability coefficient (P) and flux (Js). Figure 3 (C) shows the variability of flux according to the bentonite amount alteration. In Figure 3 (D), the limitation of prediction was shown by a mean chart of observed vs. predicted permeation coefficients of films. The film formulation (TB0) devoid of bentonite has shown highest Pfilm and Js value where the lowest has been observed films containing bentonite (TB1, TB2, TB3, TB4, TB5). Figure 3 (D) depicts the relationships between in vitro release and film permeation. The correlation coefficient 0.960–0.997 and regression equation of the in vitro release against ex vivo permeation graph are

shown in Table 4, revealing a good Level A correlation between in vitro release and ex vivo permeation. A good correlationship ensures batch-to-batch consistency in ex vivo film performance. The results revealed the influence of bentonite on the permeability coefficient. Dunnett's test study (Table 4) revealed that formulation permeation coefficients varied significantly from the control formulation (TB0) by comparing pair wise: TB0 vs TB1, TB0 vs TB2, TB0 vs TB3, TB0 vs TB4, TB0 vs TB5. The findings show that bentonite has a significant influence on the ex vivo penetration of films into ocular tissue. With decreasing bentonite ratios in formulations, the flux dropped from 60.022 to 11.045. The flux of permeation in films with different bentonite concentrations is depicted in Figure 3 (C).

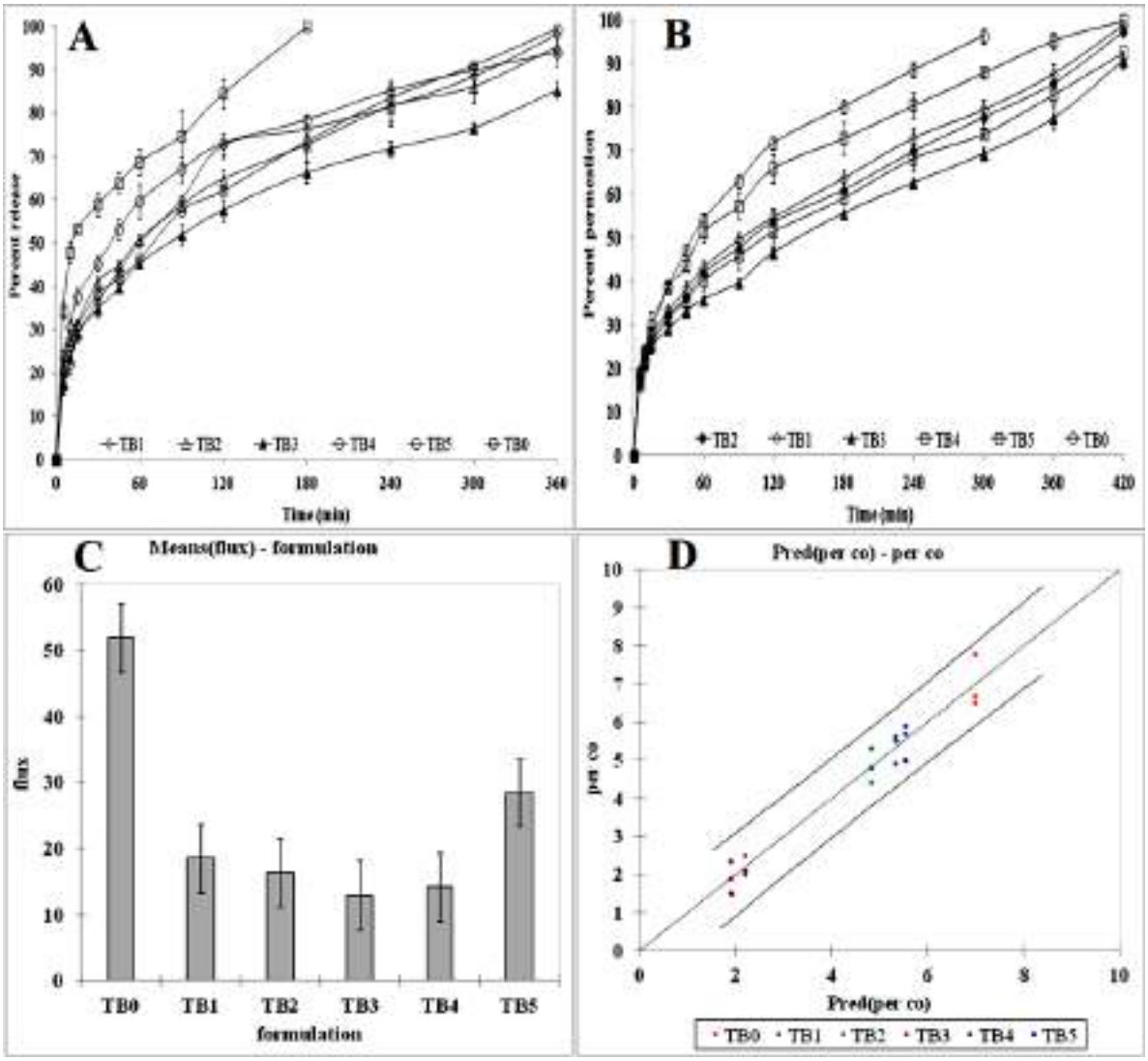

Figure 3 Dissolution (A) and Permeation profiles; (B) of trimetazidine dihydrochloride and film formulations across cornea at 34 ◦C; (C) Js (flux) as a function of bentonite content; (D) mean chart of observed vs. predicted permeation coefficient.

IOP Result

After instillation of several formulations, such as ocular trimetazidine drop (TD), film formulation without bentonite (TB0), and film formulation with bentonite the highest sustained release (TB3), the IOP reducing effects of TZ in normotensive rabbit eyes examined. The mean IOP value before the administration of TZ instillation (zero time) was (20.03 ± 0.9 mm Hg). It was observed that with 2 mg/kg (50 µl) TZ the IOP lowering effect reached the maximum value of 15.4 ± 0.7 mmHg within 120 min and the TB0 formulation reached the maximum value of 15.03 ± 0.75 mmHg within 240 min after instillation. On the other hand the IOP-lowering impact diminished and was completely abolished within 210 min and 300 min for drop and TB0 formulation respectively. In contrast, the TB3 formulation resulted in a significant and persistent decrease in IOP. TB3 demonstrated an impact that lasted up to 6 h. The peak effect of TB3 was observed at 240 min with reduction of IOP value 14.6 ± 0.8 mmHg. The area under the decreased IOP versus time curve (AUDC) was carried out after administration of different TZ formulation Figure 4 (C). The AUDC value for drop was 43.112 ± 5.06 mm Hg where as for TB0 and TB3 it was found 80.433 ± 4.816 mm Hg and 95.196 ± 5.3 mm Hg respectively. Due to the quick availability of TZ in high concentration in solution form, ocular drops of TZ had an immediate impact. But in case of TB0, TB3 was embedded or cross linked in polymer matrix, sufficient concentration of TZ was not attend to produce an immediate effect. The formulation's sustained effect could be attributable to HPMC's increased mucoadhesion in the formulation, and bentonite's synergistic effect on tissue binding in TB3. As a result, when compared to eye drops, the formulated TB3 was found to be more efficient in lowering IOP in eyes. The correlations

between amount permeated and AUDC of formulations are shown in Figure 4 (E, F). The correlation coefficient (0.9742 for TB0 and 0.984 for TB3) and regression equation of the quantity permeated versus AUDC graph are shown in the figure, indicating a good Level A correlation between ex vivo permeation and AUDC.

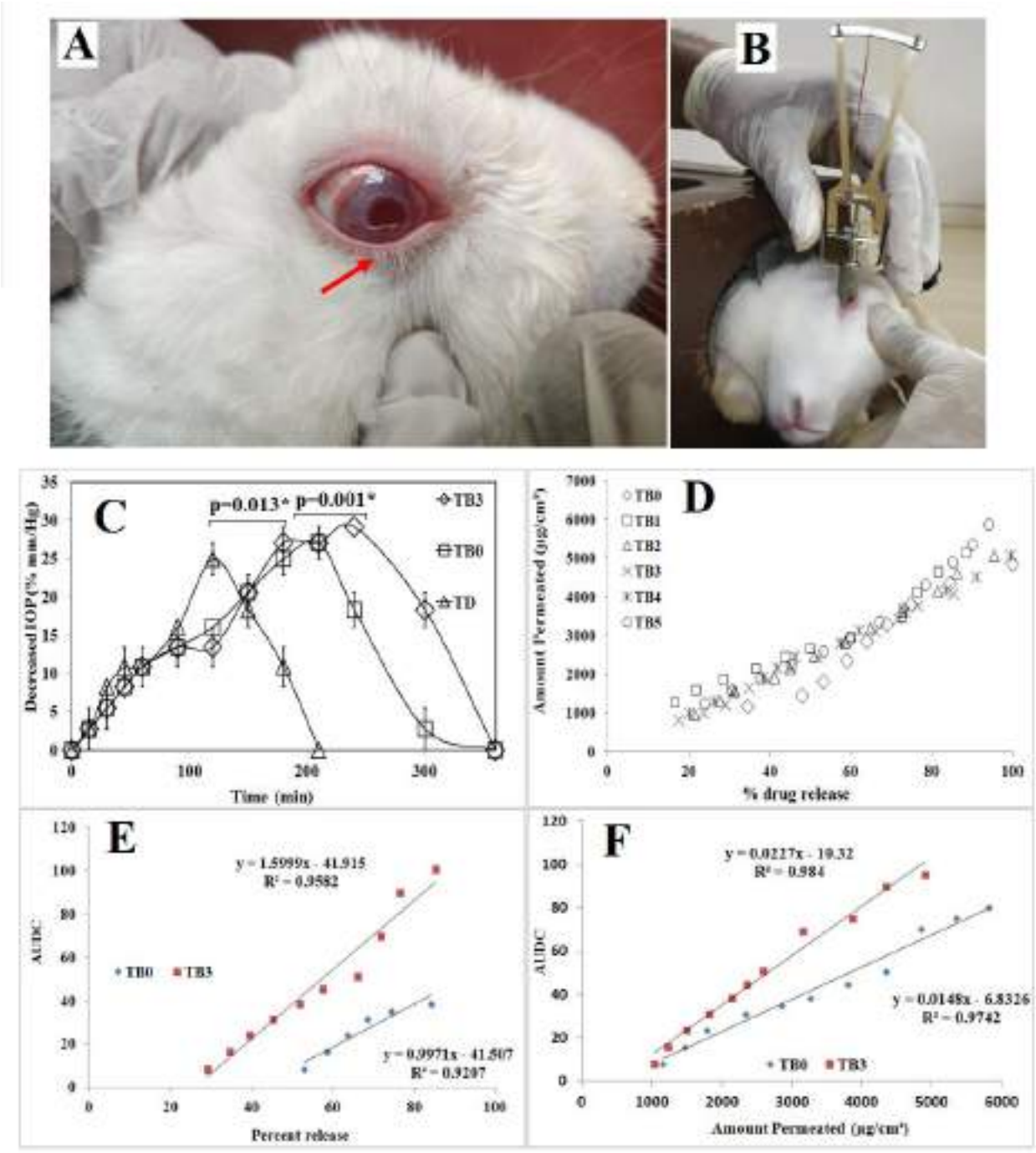

Figure 4 TZ film administred into the rabbit cul-de-sac region (A), Measuring of intra ocular pressure (IOP) by using Schiotz Tonometer (B), Area under decreased IOP curve (AUDC) on normotensive rabbits the effects of different formulations of TZ on IOP in normotensive rabbits (trimetazidine drop (TD), TB0, TB3) has shown in Figure (C) in both cases, e.g. area under decreased IOP value of the formulation TB3 is significantly higher from the ocular drop of trimetazidine ($p = 0.013$) and TBO ($p = 0.001$) at the bracketed significant level, correlation between drug release in vitro and permeability ex vivo of the film (D), Correlation between in vitro drug release and area under decreased IOP (E); Ex vivo permeation and area under decreased IOP (F).

Docking

Molecular docking is a type of artificial intelligence technique that can predict the molecular interaction of any biological substances. Docking can also confirm the fitting of a drug with a carrier with a stable configuration and a favourable energy. Therefore, we applied molecular modelling to illustrate the drug intercalated in Na-Montmorillonite. Based on the individual docking score (kcal/mol), HPMC-drug was comparability higher docking score -2.71 kcal/mol Figure 5 (A) in comparison, the montmorillonite unit cell-drug produced -1.98 kcal/mol Figure 5 (B). Concurrently, according to our objectives, 'HPMC-DRUG-UNIT CELL' obtained -5.74 kcal/mol, which indicates as a stable interaction than from a single chemical docking complex in Figure 5 (D). Thus, docking analysis can support the suitability of drug delivery and fitting of a drug with a stable configuration with favorable binding energy (van der Waals, ion-dipole, dipole-dipole interaction, H-bonding, etc.). Briefly, as per the theoretical chemistry point of view, there was an ideal embolism between polar organic molecules with hydroxyl groups of the Na-bentonite layer. The drug adsorption with Na-bentonite free surface and solidityfoundation of three-component layers with a polymer coat is expected to control the drug delivery as validated in the experimental section Figure 5 (D).

Our molecular modelling analysis revealed that trimetazidine intercalation was most likely caused by adsorption to the free surface as well as the creation of hydrogen bonds between the amine group hydrogen and the lamellar surface oxygen atom of Na-bentonite. The computational method illustrated the building blocks, binding energy and molecular interaction realistically as per our hypothesis. Moreover, bioinformatics tools were an indispensable part of early drug discovery, drug chemistry, and drug delivery analysis, theoretically (Fini et al., 2017; Swain et al., 2020).

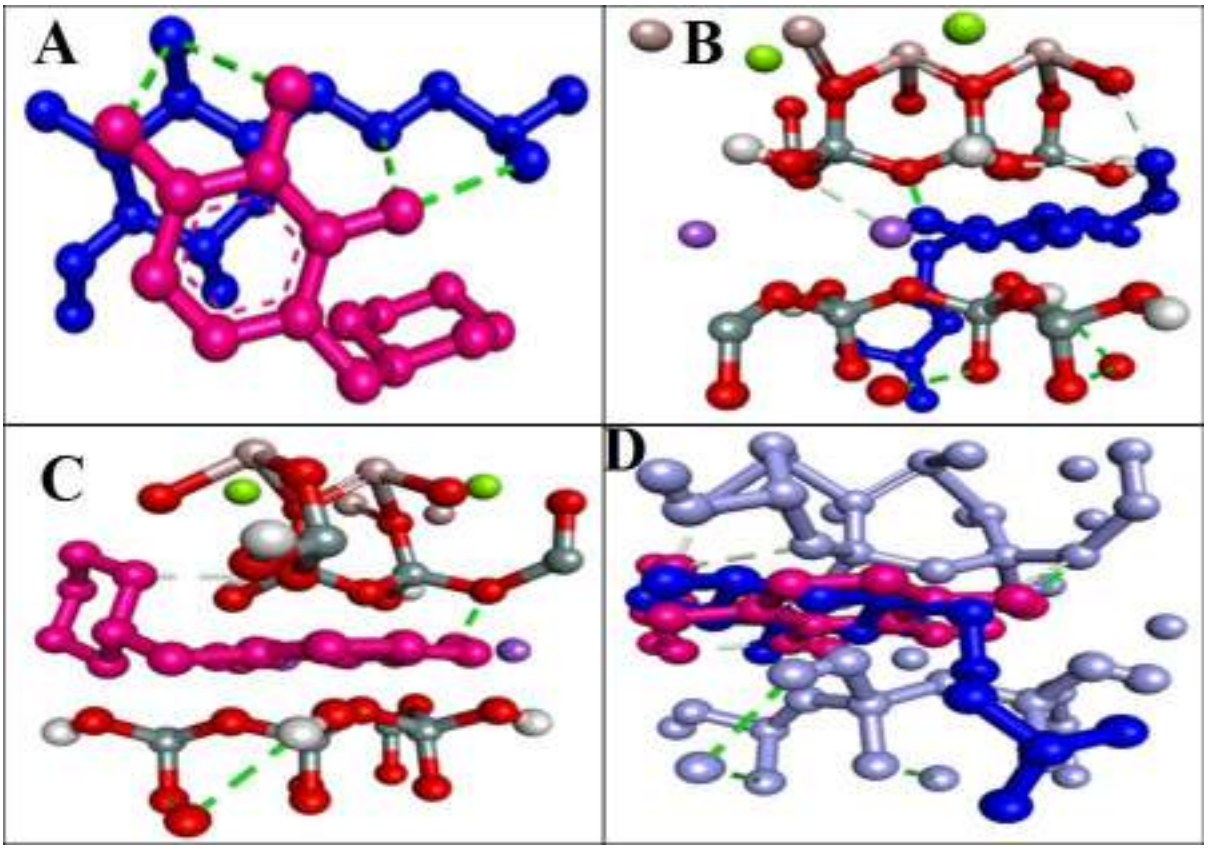

Figure 5 Molecular Docking structure of HPMC-TZ (A), HPMC-Bentonite (B), Bentonite-TZ (C), Bentonite-TZ-HPMC (D) where HPMC (Polymer – dark blue) – trimetazidine (drug-dark peach)- unit cell (montmorillonite – lavender/light purple). (For interpretation of the references to colour in this figure legend, the reader is referred to the Web version of this article.)

Objective-2

Gelling temperature, clarity and pH

A thermo-responsive system is a free-flowing sol or solution, and it forms a gel at body temperature (upon instillation in the eyes). Critical gelation temperature as the average of sol-to-gel transformation and gel-to-sol transformation of all the formulations was recorded as in the range of 32-33 °C (Figure 6) which is appropriate for in-situ-ocular gel formation upon instillation in the eye. HPMC is a suitable choice of mucoadhesive polymer for ocular delivery and the addition of HPMC in the present formulation might have improved the gelling capacity (Patel et al., 2016). Formulations were found clear, colorless, and transparent in appearance (Figure 6). The pH value was within the tolerable physiological range (6.8-7.2) of the eye.

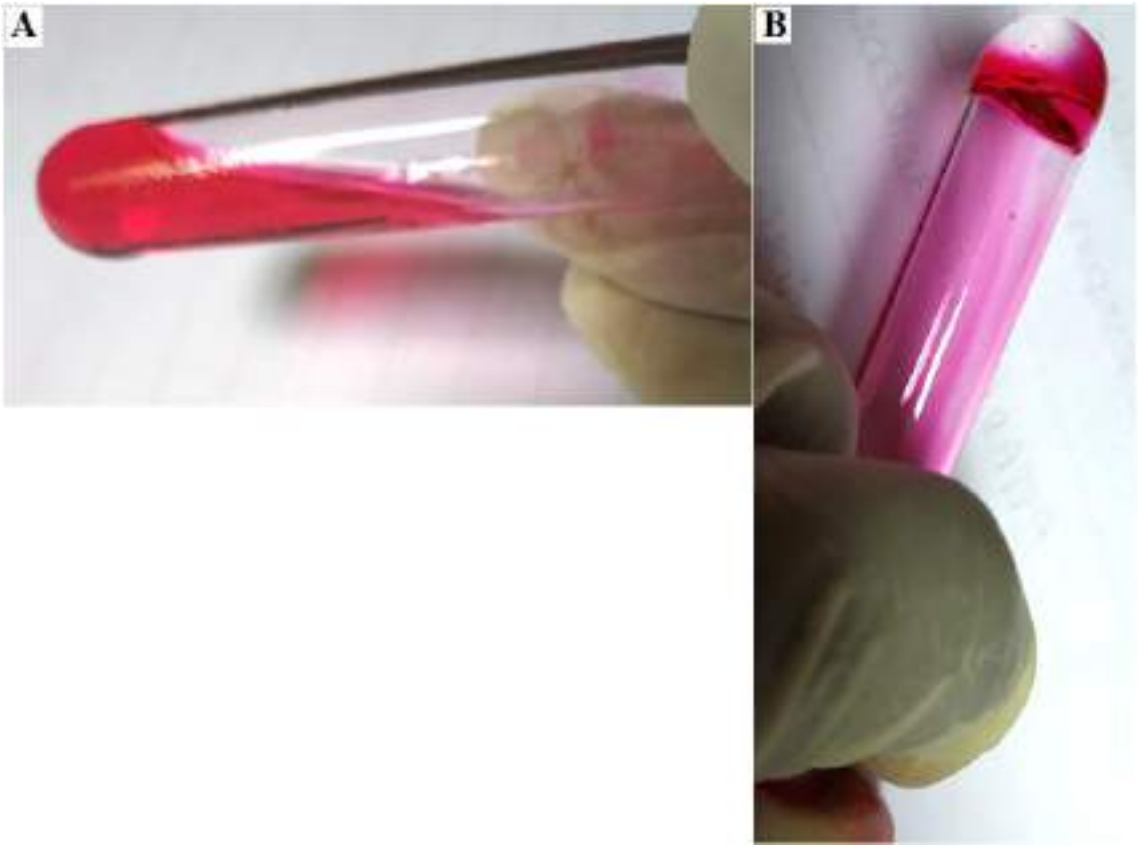

Figure 6 Gelation process of thermosensitive in-situ gel. In room temperature when the temperature is below the gelation temperature, it is clear solution with low viscosity, upon heating it to gelation temperature; the solution is converted to the gel with high viscosity.

Rheology

Rheological studies were performed at a precorneal temperature of 35 °C to describe the rheological behavior of TRZ in-situ gel formulation ($TgB_{1.0}$). Apparent viscosity has been decreased with the increase of shear rate as depicted in Figure 7 A. Shear rate vs. Shear stress flow curve (Figure 7 B) also shows the same non-Newtonian pseudoplastic shear thinning behavior starting from zero without any yield value. High viscosity at low shear rate is the positive attribute of the tolerability of the sol formulation after instillation. The pseudoplastic behavior of the developed in-situ gel allows for smooth spreading on the epithelial surface and enhanced precorneal residence duration at the same time avoiding discomfort by blinking.

To investigate the viscoelastic properties of the prepared in-situ gel under a small deformation frequency variation test was performed and shown in Figure 7 C. Oscillatory measurements allow simulating behavior of the systems at low shear, investigating the native behavior of semisolids at physiologically relevant shears. The elastic modulus (G′) and viscous modulus (G″) measured by oscillatory rheometry are proportional to the energy stored and recovered respectively in each deformation cycle at a set frequency. The formulation has shown a higher G′ value compared to G″ in the higher frequency duration (above 40 Hz). A model-independent method for comparison is based on the determination of difference factor ($f1$) and similarity factor ($f2$) ($f1 > 15$, and $f2 < 50$ signify the difference). A significant difference in between G′ and G″ was observed when compared pairwise ($f1$ value as: 17 and $f2$ value as: 30). This result indicates that the formulation has viscoelastic behavior which may facilitate the retention at the target site providing prolonged drug release. It was

also observed that G′ and G′′ prominently increased in response to an increase in oscillatory frequency above about 40 and 60 Hz, respectively.

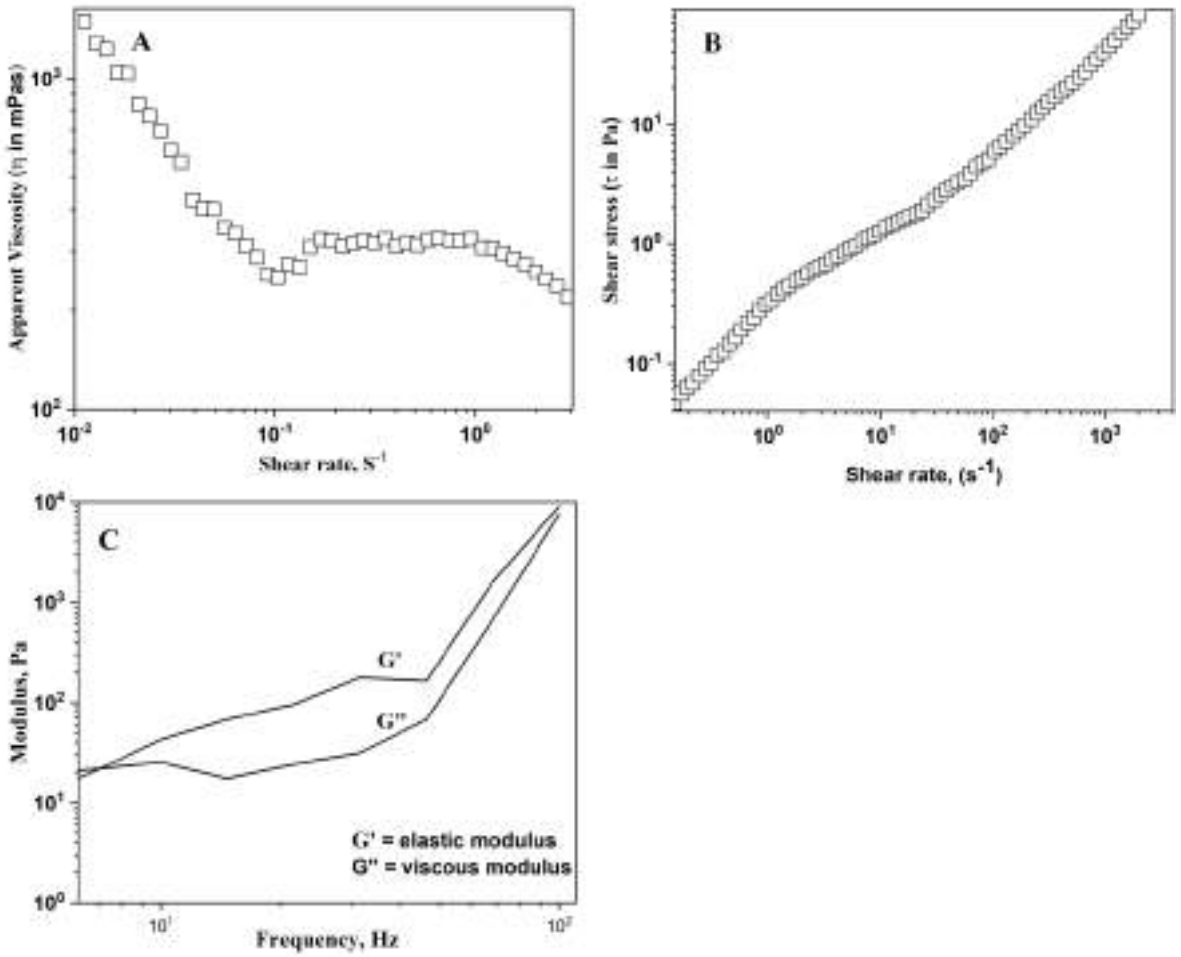

Figure 7 Apparent viscosity as a function of shear rate for TRZ in situ gel (A), Shear stress vs. shear rate flow curve (B), Elastic and viscous moduli as a function of frequency of oscillation (C).

In-vivo anti-inflammation study

Carrageenan is a well-known cytokine-mediated acute ocular inflammation model. Freund's adjuvant used to create chronic inflammation can persist up to fourteen days, but carrageenan-induced animal can be recovered in twenty four hours (Nandi et al., 2022). After 1 h of the injection of carrageenan in the eye of placebo group, watery eye with frequent lacrimation, swelling and reddening of the conjunctiva was observed (Figure 8 C). Normal eyes with no symptoms of inflammation were utilized as controls (Figure 8 B). After

treatment with $TgB_{1.0}$ prophylactically in the test group (Figure 8 D) redness has very mildly observed and inflammation has almost been vanished within 2 h (Figure 8 E).

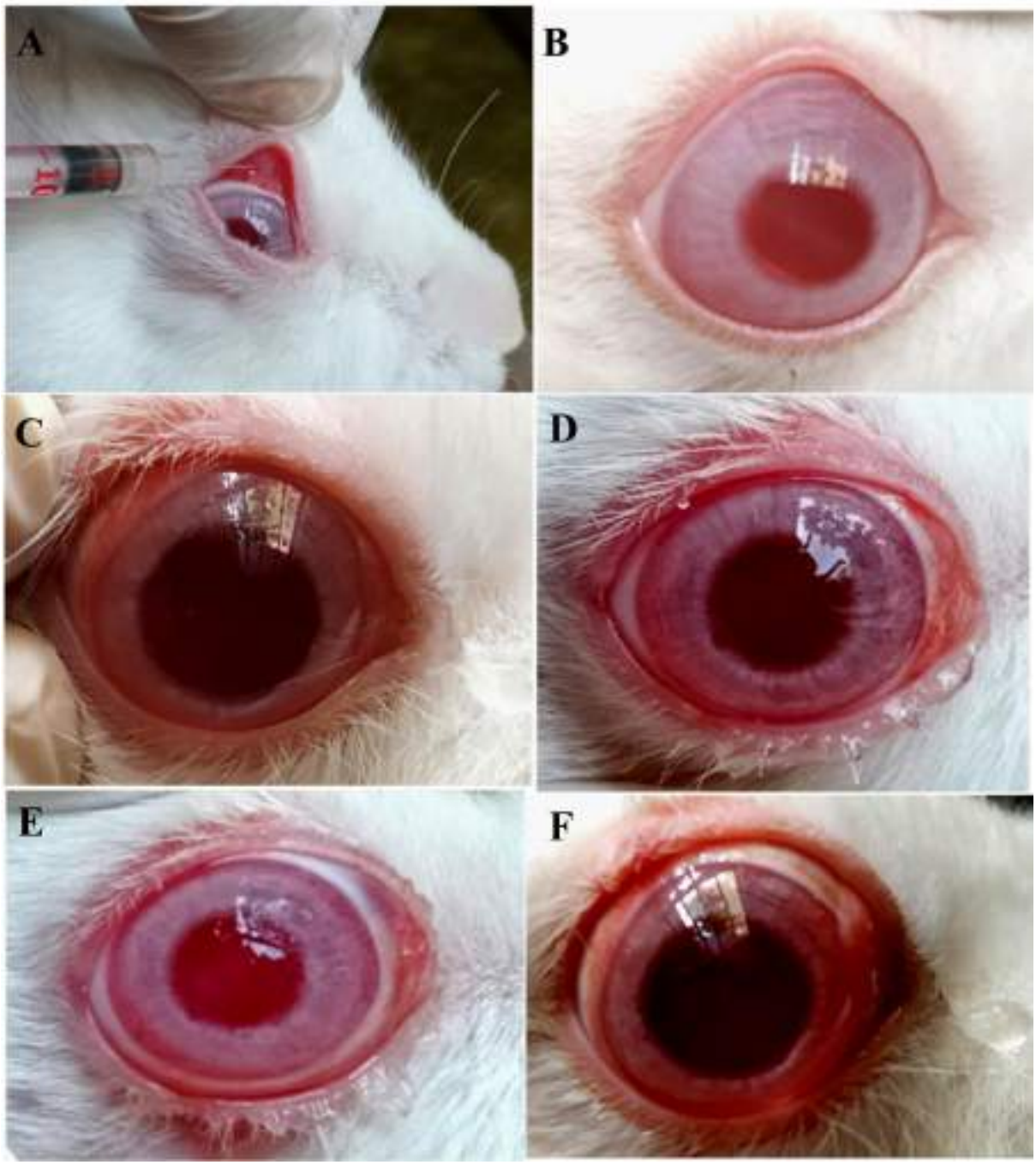

Figure 8 Carrageenan injection into the subconjunctiva of rabbit eye (A); Normal rabbit eye (B); Conjunctival redness, swelling and watery eye developed after 30 min (C); TRZ in-situ gel was applied to the cul-de-sac prophylactically, mild inflammation observed initially (D);

and after 30 min reduced inflammation (E); inflammation persisted after 2 h without applying in-situ gel (F).

Inflammatory markers such PDCD4, NF-kB, and TNF-α were shown to decrease by about 40 % after treatment with TRZ in the Guangzhou Bama miniature pig model of coronary artery micro embolism (Su et al., 2017). TRZ reduces the release of serum inflammatory mediators i.e., IL-1, IL-6, and also decreases the production of inflammatory cytokines during ischemia and inflammation (Balamurugan et al, 2020). In a report Wan et al. (2017) described that TRZ reduced caspase-8 dependent inflammatory reactions both *in vivo* and *in vitro*, which was studied by using ELISA and real time PCR (Wan et al., 2017). Anti-inflammatory effect of drug was characterized by using rabbit eye model in many published reports (Nanda et al., 2022; Pramanik et al., 2018). Prophylactic treatment with TRZ has a significant role in decreasing inflammatory cytokine TNF-α, IL-1β and ROS production in the eye, and is likely the reason of reducing the course of ocular inflammation (Wan et al., 2017).

Work in progress and suggested outcomes

- Effect of bentonite clay on the swelling of the polymeric ocular film will be studied.
- Hydration could better explain using some modified kinetic models.
- Mechanical properties like Tensile strength, strain at break, % elongation, Young's modulus (elastic modulus), and the ratio of tensile strength to Young's modulus will also be evaluated for film formulation.
- Texture profile, muco-adhesiveness and spreadability of all in situ gel formulation will be studied.
- In a report trimetazidine decreased the production of free radicals and protected smocking induced left ventricular damage (Zhou et al., 2012). That report encouraged us to study the cytoprotective role of trimetazidine in the rat eye model applying hydrogel based film formulation.
- Thiobarbituric acid reactive substance assay (TBARS) (using rat eye homogenate) and histology study of the ocular tissue will be performed to assess the cytoprotective effect.

- Increased reactive oxygen species and antioxidant defficiency are the vital causes of the pathogenesis of cataract formation in chronic diabetic condition (Sharma et al., 2020).
- Anti-cataract activity will also be performed in vitro using isolated goat eye lens collected from local butcher shop. And further in vivo study will be accomplished in selenite induced suckling rats.
- Protein content of the induced isolated rat eye lens will be carried out as per Lowry et al.,(1951).

Impact of the research in the advancement of knowledge or benefit to mankind

It is anticipated that the outcome of this project will provide a major advancement in ocular drug delivery systems (ODDSs) and will have far-reaching implications in developing novel ocular drug delivery systems. This projects finding will expand our knowledge of polymer/clay nanocomposite potential for ocular drug delivery and pave the road for the creation of next-generation ODDSs. Moreover, the management of IOP, inflammation, and cataract has the potential to significantly advance knowledge, improve therapeutic strategies, and ultimately benefit individuals suffering from ocular conditions by providing targeted, efficient, and safe treatment options.

Literature reference

1. Hironaka, K., Inokuchi, Y., Fujisawa, T., Shimazaki, H., Akane, M., Tozuka, Y., Tsuruma, K., Shimazawa, M., Hara, H., Takeuchi, H., 2011. Edaravone-loaded liposomes for retinal protection against oxidative stress-induced retinal damage. European Journal of Pharmaceutics and Biopharmaceutics 79, 119-125.
2. Masuda, T., Shimazawa, M., Hara, H., 2017. Retinal diseases associated with oxidative stress and the effects of a free radical scavenger (Edaravone). Oxidative medicine and cellular longevity 2017.
3. Durand, M.L., 2015. 117-Infectious causes of uveitis. Mandell, Douglas, and Bennett's principles and practice of infectious diseases, 8th edn. WB Saunders, 1423-1431.
4. Hu, C.-C., Liao, J.-H., Hsu, K.-Y., Lin, I.-L., Tsai, M.-H., Wu, W.-H., Wei, T.-T., Huang, Y.-S., Chiu, S.-J., Chen, H.-Y., 2011. Role of pirenoxine in the effects of catalin on in vitro ultraviolet-induced lens protein turbidity and selenite-induced cataractogenesis in vivo. Molecular vision 17, 1862.
5. Tezel, G., 2021. Multifactorial pathogenic processes of retinal ganglion cell degeneration in glaucoma towards multi-target strategies for broader treatment effects. Cells 10, 1372.
6. Rosenthal, R., Fromm, M., 2011. Endothelin antagonism as an active principle for glaucoma therapy. British journal of pharmacology 162, 806-816.
7. Choritz, L., Machert, M., Thieme, H., 2012. Correlation of endothelin-1 concentration in aqueous humor with intraocular pressure in primary open angle and

pseudoexfoliation glaucoma. Investigative ophthalmology & visual science 53, 7336-7342
8. Zhang, X., Krishnamoorthy, R.R., Prasanna, G., Narayan, S., Clark, A., Yorio, T., 2003a. Dexamethasone regulates endothelin-1 and endothelin receptors in human non-pigmented ciliary epithelial (HNPE) cells. Experimental eye research 76, 261-272.
9. Rigosi, E., Ensini, M., Bottari, D., Leone, P., Galli-Resta, L., 2010. Loss of retinal capillary vasoconstrictor response to Endothelin-1 following pressure increments in living isolated rat retinas. Experimental eye research 90, 33-40.
10. Mohand-Said, S., Jacquet, A., Lucien, A., Espinasse-Berrod, M., Frasson Correa De Silva, M., Sahel, J., 2002. Protective effect of trimetazidine in a model of ischemia-reperfusion in the rat retina. Ophthalmic Research 34, 300-305.
11. Nowak, M.S., Wybór, K., Goś, R., Zeman-Miecznik, A., Waszczykowska, A., Pastuszka, M., Kłysik, A., Gajdowska, A., 2007. Protective effect on visual functions of long-term use of trimetazidine in treatment of primary open angle glaucoma and degenerative myopia. Archives of Medical Science 3, 152-156.
12. Abdeen, R., Salahuddin, N., 2013. Modified chitosan-clay nanocomposite as a drug delivery system intercalation and in vitro release of ibuprofen. Journal of Chemistry 2013.
13. Alshabanat, M., Al-Arrash, A., Mekhamer, W., 2013. Polystyrene/montmorillonite nanocomposites: study of the morphology and effects of sonication time on thermal stability. Journal of Nanomaterials 2013, 9-9.
14. Fini, E.H., Høgsaa, B., Christiansen, J.d.C., Sanporean, C.-G., Jensen, E.A., Mousavi, M., Pahlavan, F., 2017. Multiscale investigation of a bioresidue as a novel intercalant for sodium montmorillonite. The Journal of Physical Chemistry C 121, 1794-1802.
15. Swain, R., Nandi, S., Sahoo, R.N., Swain, S.S., Mohapatra, S., Mallick, S., 2022. Bentonite clay incorporated topical film formulation for delivery of trimetazidine: Control of ocular pressure and in vitro-in vivo correlation. Journal of Drug Delivery Science and Technology 67, 102956.
16. Chiş, A., Kacsó, I., Borodi, G., Bratu, I., 2011. COMPLEXUL DE INCLUZIUNE AL TRIMETAZIDINEI CU β-CYCLODEXTRINA. Clujul Medical 84.
17. Zhang, H., Shi, Y., Xu, X., Zhang, M., Ma, L., 2020. Structure regulation of bentonite-alginate nanocomposites for controlled release of imidacloprid. ACS omega 5, 10068-10076.
18. Savas, L.A., Hancer, M., 2015. Montmorillonite reinforced polymer nanocomposite antibacterial film. Applied Clay Science 108, 40-44.
19. Chang, P.-H., Jiang, W.-T., Sarkar, B., Wang, W., Li, Z., 2019. The triple mechanisms of atenolol adsorption on ca-montmorillonite: Implication in pharmaceutical wastewater treatment. Materials 12, 2858.
20. Hosseini, F., Hosseini, F., Jafari, S.M., Taheri, A., 2018. Bentonite nanoclay-based drug-delivery systems for treating melanoma. Clay Minerals 53, 53-63.
21. Patel, N., Thakkar, V., Metalia, V., Baldaniya, L., Gandhi, T., Gohel, M., 2016. Formulation and development of ophthalmic in situ gel for the treatment ocular inflammation and infection using application of quality by design concept. Drug development and industrial pharmacy 42, 1406-1423.
22. Nandi, S., Ojha, A., Nanda, A., Sahoo, R.N., Swain, R., Pattnaik, K.P., Mallick, S., 2022. Vildagliptin plasticized hydrogel film in the control of ocular inflammation after topical application: study of hydration and erosion behaviour. Zeitschrift für Physikalische Chemie 236, 275-290.

23. Su, Q., Li, L., Zhao, J., Sun, Y., Yang, H., 2017. Effects of trimetazidine on PDCD4/NF-κB/TNF-α pathway in coronary microembolization. Cellular Physiology and Biochemistry 42, 753-760.
24. Balamurugan, S., Das, D., Hasanreisoglu, M., Toy, B.C., Akhter, M., Anuradha, V., Anthony, E., Gurnani, B., Kaur, K., 2020. Interleukins and cytokine biomarkers in uveitis. Indian Journal of Ophthalmology 68, 1750.
25. Wan, P., Su, W., Zhang, Y., Li, Z., Deng, C., Zhuo, Y., 2017. Trimetazidine protects retinal ganglion cells from acute glaucoma via the Nrf2/Ho-1 pathway. Clinical Science 131, 2363-2375.
26. Nanda, A., Das, S., Sahoo, R.N., Nandi, S., Swain, R., Pattanaik, S., Das, D., Mallick, S., 2022. Aspirin–hydrogel ocular film for topical delivery and ophthalmic anti-inflammation. Journal of the Serbian Chemical Society 87, 829-843.
27. Pramanik, A., Sahoo, R., Nanda, A., Pattnaik, K., Mallick, S., 2020. Swelling kinetics and corneal hydration level of Kaolinin-HPMC hydrogel film. Indian Journal of Pharmaceutical Sciences 82, 306-314.

Candidate Signature